FOI
SWEDISH DEFENCE
RESEARCH AGENCY

FOI-R--1191--SE
February 2004
ISSN 1650-1942
Technical report

Jan Svedin, Lars-Gunnar Huss

A 94 GHz imaging radar system

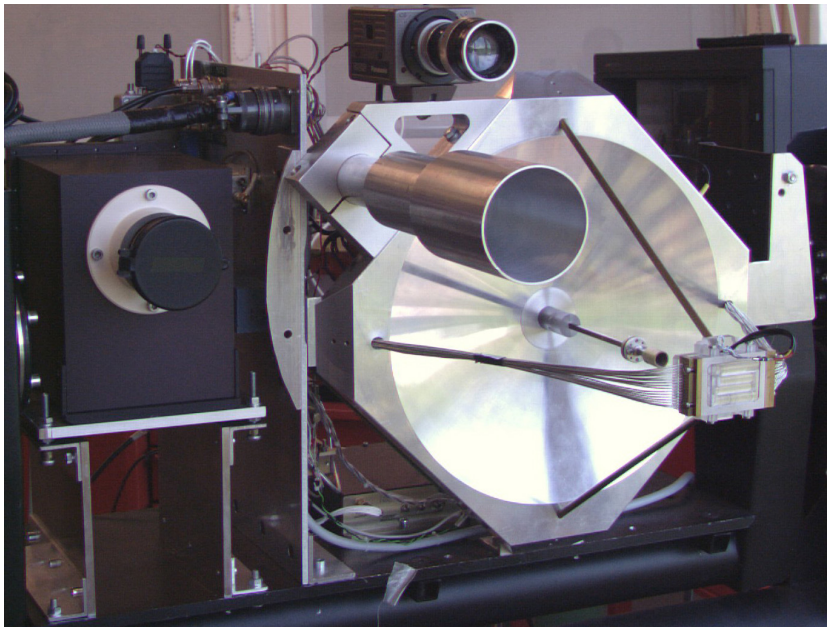

Sensor Technology
SE-581 11 Linköping

SWEDISH DEFENCE RESEARCH AGENCY

Sensor Technology
P.O. Box 1165
SE-581 11 Linköping

FOI-R--1191--SE

February 2004

ISSN 1650-1942

Technical report

Jan Svedin, Lars-Gunnar Huss

A 94 GHz imaging radar system

Issuing organization	Report number, ISRN	Report type
FOI – Swedish Defence Research Agency Sensor Technology P.O. Box 1165 SE-581 11 Linköping Sweden	FOI-R--1191--SE	Technical report
	Research area code 5. Combat	
	Month year February, 2004	**Project no.** E3062
	Customers code 5. Commissioned Research	
	Sub area code 51 Weapons and Protection	

Author/s (editor/s)	Project manager
Jan Svedin Lars-Gunnar Huss	Leif Carlsson
	Approved by Hans Frennberg
	Sponsoring agency FM
	Scientifically and technically responsible Jan Svedin

Report title

A 94 GHz imaging radar system

Abstract (not more than 200 words)

This report describes the 94 GHz imaging radar system that has been developed and used within the IR/mm project during the years 2001-2003. The new system, which is based on active gate mixers (GaAs MMIC), shows higher performance than an earlier used system, which was based on resistive mixers (InP HEMT). The conversion loss and pumping power requirement have both been reduced which has resulted in a significant improvement of the system sensitivity. A measured SNR of about 3 dB has been obtained (in average over 4x8 channels) for a 1 m^2 target at a 500 m measurement distance.

Keywords

Mm-wave, focal plane arrays, MMIC, antennas, multisensortechnique, missile seeker

Further bibliographic information	Language English
ISSN 1650-1942	**Pages** 40 p.
	Price acc. to pricelist

Utgivare	Rapportnummer, ISRN	Klassificering
Totalförsvarets Forskningsinstitut - FOI Sensorteknik Box 1165 581 11 Linköping	FOI-R--1191--SE	Teknisk rapport
	Forskningsområde 5. Bekämpning	
	Månad, år Februari, 2004	**Projektnummer** E3062
	Verksamhetsgren 5. Uppdragsfinansierad verksamhet	
	Delområde 51 VVS med styrda vapen	

Författare/redaktör	Projektledare
Jan Svedin Lars-Gunnar Huss	Leif Carlsson
	Godkänd av Hans Frennberg
	Uppdragsgivare/kundbeteckning FM
	Tekniskt och/eller vetenskapligt ansvarig Jan Svedin

Rapportens titel (i översättning)

Ett 94 GHz bildalstrande radarsystem

Sammanfattning (högst 200 ord)

Denna rapport beskriver det 94 GHz bildalstrande radarsystem som har utvecklats och använts inom IR/mm-projektet under åren 2001-2003. Det nya systemet, som är baserat på aktiva gateblandare (GaAs MMIC), uppvisar högre prestanda än ett tidigare framtaget system, som var baserat på resistiva blandare (InP HEMT). Konversionsförlusten och behovet av LO-effekt har båda reducerats vilket har resulterat i en signifikant förbättring av systemkänsligheten. Ett uppmätt SNR på omkring 3 dB har erhållits (i medel över 4x8 kanaler) för ett 1 m^2 mål på 500 m mätavstånd.

Nyckelord

Mm-våg, fokalplansarray, MMIC, antenner, multisensorteknik, målsökare

Övriga bibliografiska uppgifter	Språk Engelska
ISSN 1650-1942	**Antal sidor:** 40 s.
Distribution enligt missiv	**Pris: Enligt prislista**

FOI1004 Utgåva 11 2002.02 www.signon.se Sign On AB

Contents

1. Introduction

This report presents the new 94 GHz imaging (4x8) radar system that has been developed within the IR/mm-project during the years 2001-2003.

The new system uses a front-end based on active gate mixers (GaAs MMIC) with improved performance compared to an earlier developed system that used a front-end based on resistive mixers (InP HEMT). The conversion loss and the pumping power requirement have both been reduced which results in a significant increase in the overall performance.

Aside from using a new millimeterwave front-end (a new mixer and different antenna circuits) and a modified IF-stage, the new system uses the same parabolic reflector setup as the earlier developed (4x4 pixels) system.

The report also reports on some new antenna designs that have the potential to further improve the performance of the radar.

2. Focal plane array

The principle of a focal plane array (FPA) is shown in Fig. 2.1. An antenna array is placed in the focal plane of a lens/reflector with diameter D and focal length F. The field of view is approximately given by $W \approx x/F$, where x is the diameter of the FPA.

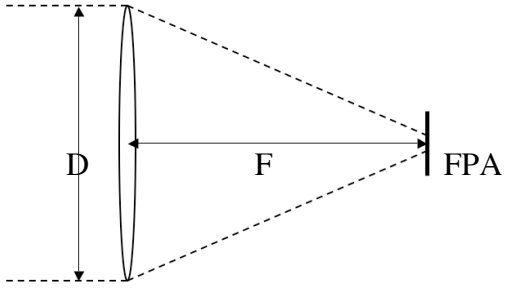

Fig. 2.1. Principle of an FPA

The lens/reflector antenna has an angular resolution of $\Delta\theta \approx \lambda/D$. If an antenna array is placed in the focal plane of a lens and has an element spacing of $d \leq \lambda(F/D)$ the angular resolution will be diffraction limited. In general the angular resolution for an FPA is given by

$$\Delta\theta \approx \max\left(\frac{d}{F};\frac{\lambda}{D}\right) \tag{E.1}$$

More accurately the distance between adjacent elements should be chosen so that the Nyquist sampling criterion [1] is fulfilled,

$$d \leq \frac{f\lambda}{pn} \tag{E.2}$$

where n is the refractive index for the material in which the image is formed, p is 1 and 2 for coherent and non-coherent detection, respectively, and the f-number f=F/D. More accurately the far-field scan angle, θ, for a primary-fed parabolic reflector as a function of the displacement d in the focal plane is given by [2] (and references therein)

$$\theta = \mathrm{BDF} \cdot \mathrm{atan}\left(\frac{d}{F}\right) \tag{E.3}$$

where BDF is the so-called beam deviation factor, which is a function of the f-number. For a fixed element spacing the focal length needs to be determined so that the element spacing corresponds to a far-field scan angle of approximately one beamwidth, i.e., the main beams should overlap at the –6 dB points if full coverage is required.

To optimize system performance it is of importance to match the feed antenna beamwidth to the f-number of the system. Typical values of optimum feed taper are in the range of –10 to –13 dB [3]. The –10 dB beamwidth, θ_{-10dB}, of the antenna element should match the opening angle, θ_0, of the reflector. If $\theta_{-10dB} >> \theta_0$ spillover loss (SPL) will occur. If $\theta_{-10dB} << \theta_0$ amplitude taper loss (ATL) and phase error loss (PEL) will occur as a result of deviations from constant amplitude and phase in the aperture field.

The current antenna system is a primary-fed parabolic reflector with a diameter of 30 cm and a FPA consisting of 4x8 antenna elements. The 4x8 FPA allows scan angles of up to approximately 2.5° x 5.0°. An expression is given in [3] for the maximum number of beamwidths that can be scanned if a 1 dB gain loss can be tolerated

$$n_{max} = 0.44 + 22\left(\frac{F}{D}\right)^2 \qquad \text{(E.4)}$$

Eq. 4 assumes a –10 dB edge taper. The maximum number of beamwidths that can be scanned with the current system is 16.

Design of the reflector antenna system is described in [2] and the resulting parameters of interest are presented in Table 1. The radiation efficiency of the microstrip antennas at 94 GHz is 50-60 % which adds a loss of 2-3 dB to the system.

f=F/D	DIR [dB]	θ_{3dB}	SPL, ATL, PEL [dB]	Gain [dB]
5/6	49	0.7°	4 (mainly from SPL)	42-43

Table 1. Calculated parameters for the reflector antenna system.

In Fig. 2.2 measured co-polarization patterns for eight sensors are plotted. The beamwidth is approximately 0.6° with a maximum relative sidelobe level of –12 dB. The distance between adjacent beams is approximately 0.7°.

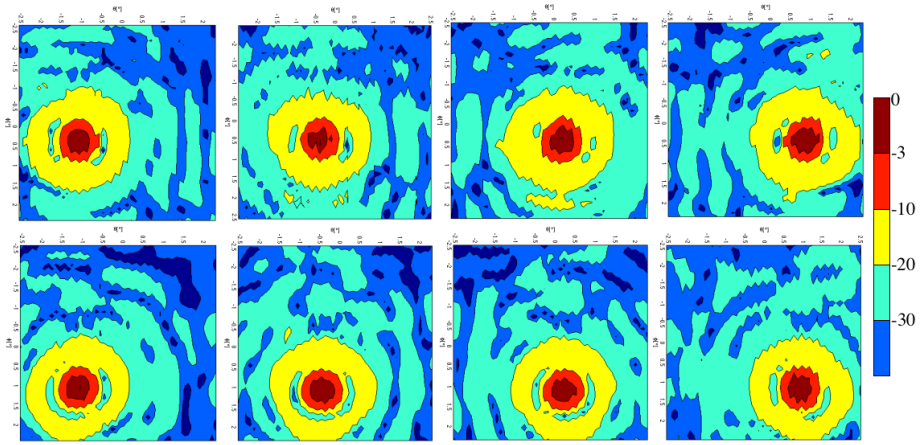

Fig. 2.2. Contours of measured copol patterns for eight sensors.

2.1. Radar system

The radar system is a 94 GHz imaging pulse radar system comprising 4x8 pixels with 4 pixels coverage in elevation and 8 pixels in azimuth. The resulting field of view is approximately 2.5° in elevation and 5° in azimuth.

The reflector system uses a primary-fed parabolic reflector with a 30 cm reflector and an f-number of 5/6, which earlier was found optimal for this application [2]. The reflector beamwidth is approximately 0.7° and the gain was earlier calculated and measured both to be in the range 42 to 43 dB depending on the distance from the optical axis (scan loss).

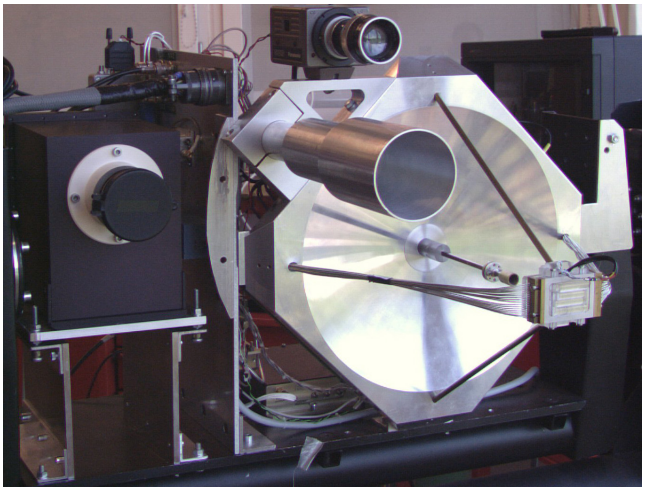

Fig. 2.1.1. Photo of reflector system with the 4x8 focal plane array. The LO signal is illuminated quasi-optically using a scalar horn located at the center of the reflector. The large circular horn is the transmit antenna.

The radar transmits 50 ns pulses with a peak power of 10 W (with an adjustable PRF, 10-50 kHz) from the circular horn in the upper left of Fig. 2.1.1. The calculated 3 dB beamwidth and gain of the transmit horn is approximately 5° and 30 dBi, respectively. The millimeter-wave radar together with a video camera and an IR-camera are mounted on a platform that can be scanned mechanically in both azimuth and elevation. The generation of the RF pulse and LO signal is described elsewhere.

A photo showing how the IF cards are mounted on the backside of the reflector is given in Fig. 2.1.2. In the figure it can also be seen how a waveguide is used to connect the LO source (bottom right corner) to the LO scalar horn antenna.

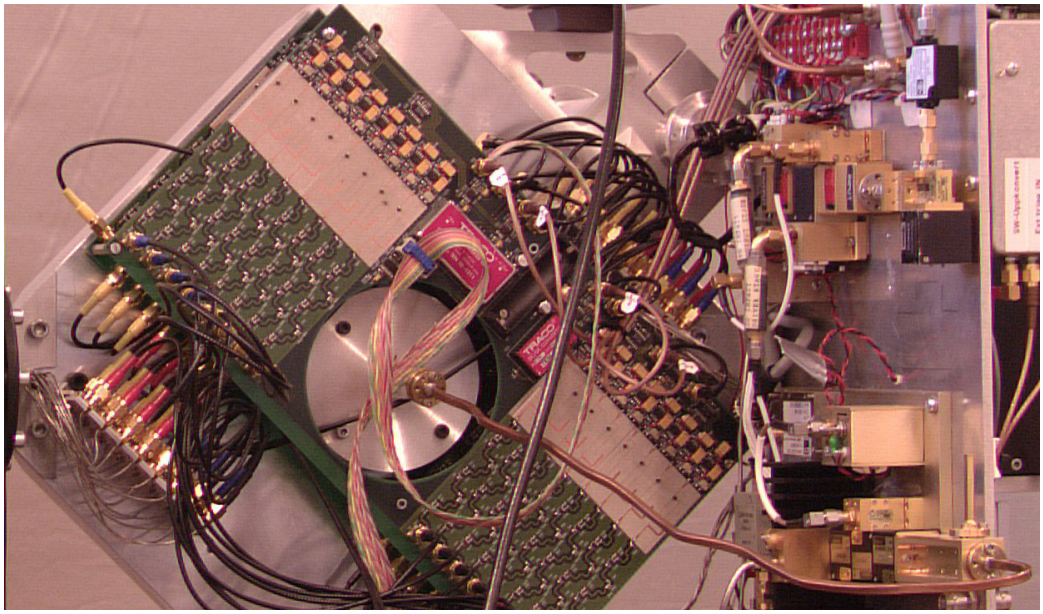

Fig. 2.1.2. Photo showing the IF cards mounted on the backside of the reflector.

2.2. Front-end

The 4x8 system is assembled using two FPA chips, each of dimensions 20 mm x 20 mm, giving a total chip size of 40 mm x 20 mm. The chip fixture dimension is 50 mm x 40 mm. A CAD layout of the two subarrays is shown in Fig. 2.2.1 and a photo of the chip fixture is given in Fig. 2.2.2, which shows two struts and the 4x8=32 IF (miniature semi-rigid) cables.

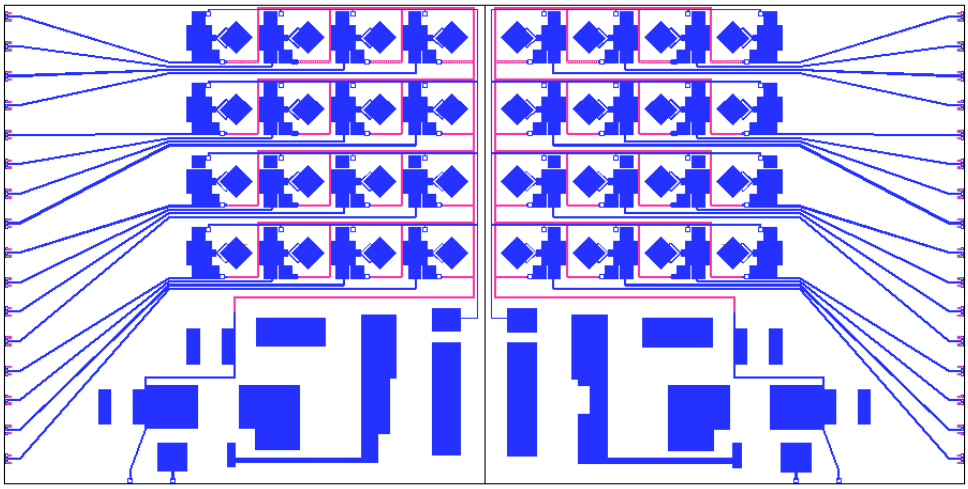

Fig. 2.2.1. Shows CAD layout of the antenna circuit used for the 4x8 radar system. Two different antenna chips are used with a mirrored version of the mixer on the right antenna chip.

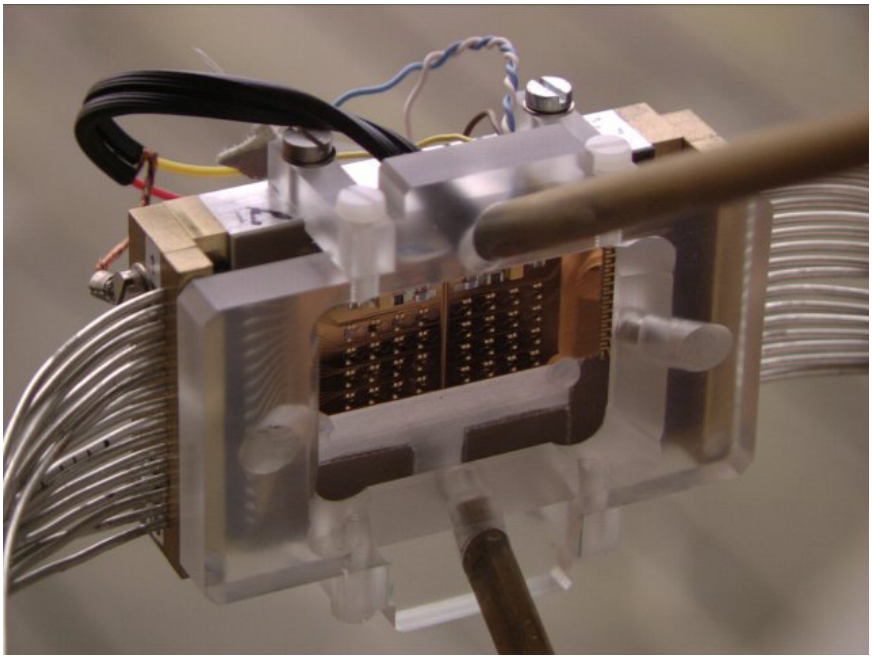

Fig. 2.2.2. Photo of focal plane array chip fixture. The dimensions are 50 mm x 40 mm. The down-converted IF signals are distributed to the IF-cards at the backside of the reflector using miniature semi-rigid cables.

Microstrip-fed rectangular patch antennas of dimensions 960 mm x 942 mm with dual feeds are utilized to receive the RF and LO in orthogonal polarizations in each channel. A close-up photo of one sensor is shown in Fig. 2.2.3. The LO signal is transmitted quasi-optically to all channels from a scalar horn antenna positioned approximately 8 cm from the sensor array.

The gate and drain bias voltages are supplied simultaneously to filter and protection networks located on each of the two antenna chips and distributed using DC lines routed in the two uppermost metal layers of the multi-chip module (MCM). External decoupling capacitors for the gate and drain bias are used in conjunction with smaller on-chip capacitors. The IF signals are routed using microstrip lines through coupling capacitors to the edge of the chips. Transitions from microstrip to CPW pads are then used to transfer the 1.6 GHz IF signals to an external FR-4 substrate.

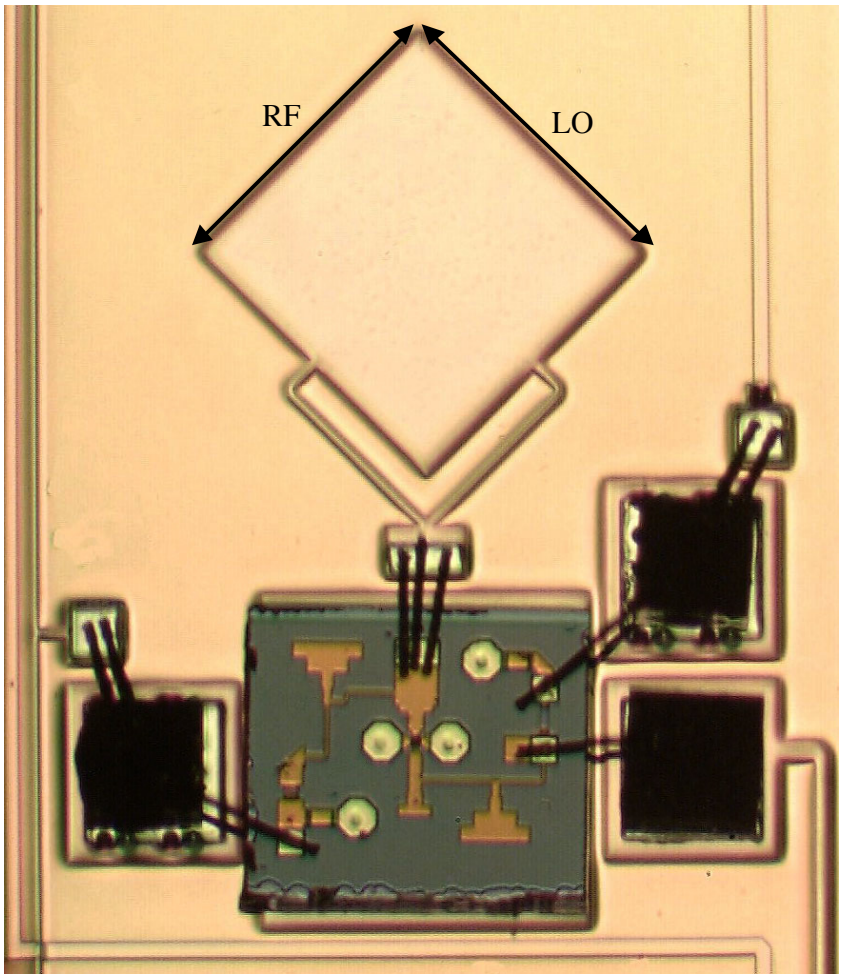

Fig. 2.2.3. Photo of single sensor element with dually polarized patch antenna with mounted active gate mixer MMICs

Each sensor uses a 2 x 25 μm active gate mixer with dimensions 1 x 1 mm^2, described in chapter 3. The RF and LO are extracted from neighboring sides of the patch and combined at the

gate of the mixer. The antenna is matched to the mixer gate input taking into consideration the parasitic effects of the bond wires. Three wires in parallel are used to minimize the inductance. The mixer was measured and found to give a minimum conversion loss of approximately 3.7 dB in a 50 Ω system using an LO power of roughly 0 dBm. By measuring the mixer input impedance using a HP8510XF VNA a matched conversion loss (after subtracting the impedance mismatch loss) of around 0.5 dB could be calculated (using a matched LO power of approximately –2 dBm).

The measured impedance of the mixer was also used to calculate the mismatch loss between mixer and antenna for the circuit in Fig. 2.2.3. The calculated mismatch loss, plotted in Fig. 2.2.4, is between 2 and 3 dB in the frequency range 92.4 GHz to 94 GHz, i.e., there is a potential for improvement using a better matching circuitry. See more details in Chapter 3.

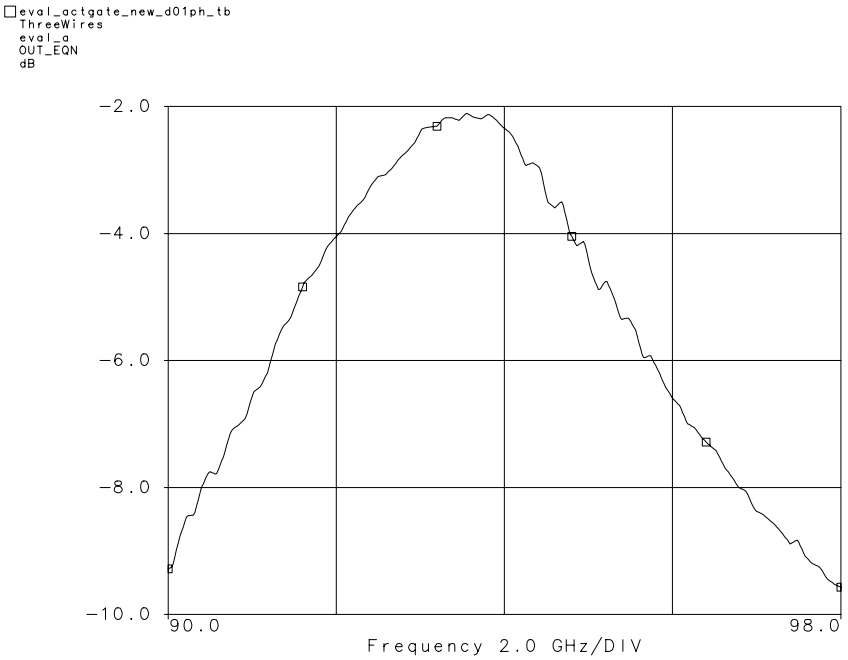

Fig. 2.2.4. Shows the calculated mismatch loss for the new sensor using the measured impedance of the mixer and calculated impedance of the patch antenna (HP Momentum).

2.3. IF-circuits

The IF-circuit card for the 4x8 system is based on the card that was developed in-house for the older 4x4 system. It contains IF amplifiers (35 dB gain, NF < 2 dB), filters, diode detectors,

video amplifiers and multiplexers. The card is manufactured on a FR-4 substrate and assembled at FOI. The diode matching circuitry is based on open stubs and transmission line sections.

A problem with the previous card was a too low center frequency for the diode matching circuitry. This was caused by a relative permittivity of the FR-4 substrate differing from the specified value used for the design. Because it was found impossible to obtain accurate values for the relative permittivity the new card instead uses a matching circuit manufactured on a separate RT Duroid 6010 substrate. This Duroid card is glued using conductive glue to mounting pads on the FR-4 card, see Fig. 2.3.1. In this way it was possible to obtain a match of the diode to the amplifier output at 1.6 GHz with a ±50 MHz bandwidth (at low input levels to the diode detector). An optional tuning capability was included using slightly longer stubs than was calculated for the optimal match. An open stub is also used at the output of the detector diode because the impedance of the video circuitry impedance is difficult to measure/simulate at 1.6 GHz. The impedance of this stub is much higher at the highest video frequency (50 MHz) compared to the input impedance of the video amplifier.

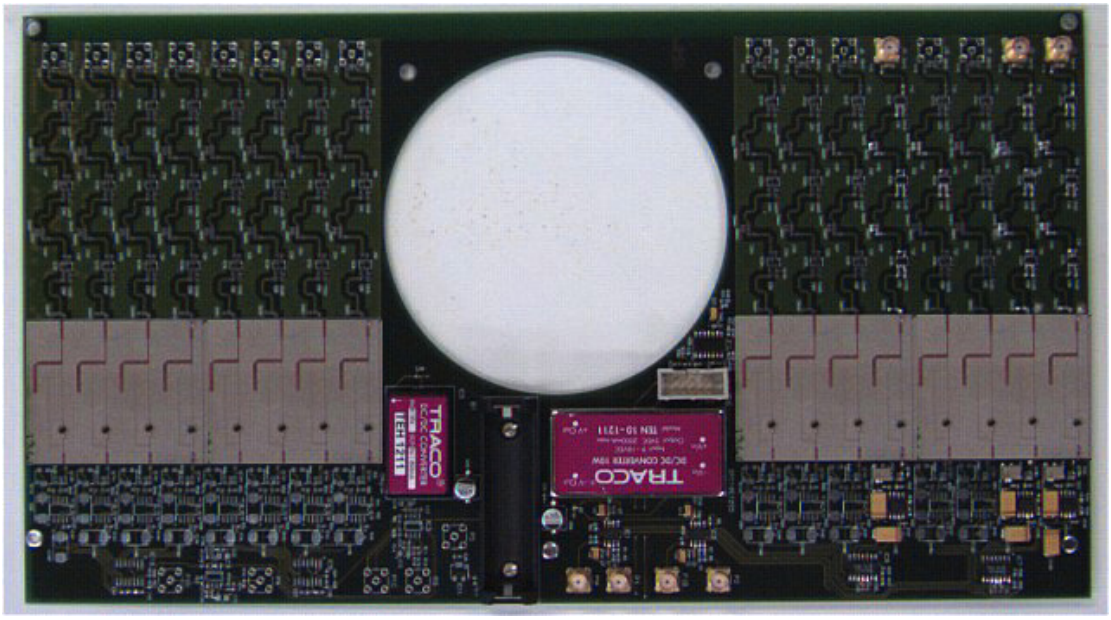

Fig. 2.3.1. Photo of the IF-circuit card with diode matching circuit manufactured on a separate Duroid substrate (grey/white) which is glued to the multilayer FR-4 card (green).

The tangential sensitivity (TSS) of the diode (HP HSMS-285B), i.e., the lowest signal power level for which the detector will have a 4 dB SNR at the output of the video, was measured by

using a cw signal at 1.6 GHz. This signal was pulse modulated with 50 ns rectangular pulses and a pulse repetition frequency (prf) of 20 kHz. The TSS for the diode was measured to –48 ± 2 dBm and the output dynamic range of the detector is about 30 dB (voltage), see Fig 2.3.2.

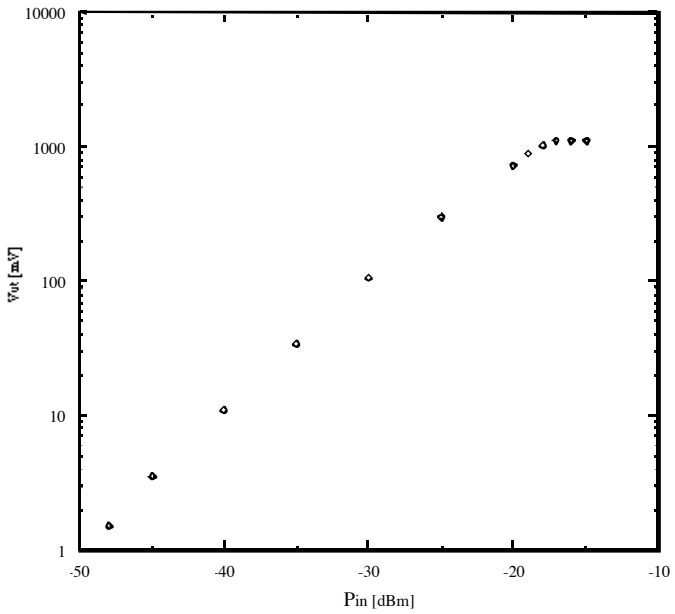

Fig. 2.3.2. Detector response versus input power for a pulsed signal t = 50 ns, PRF = 20 kHz.

2.4. Measured system performance

The performance of the system was measured mainly by obtaining the conversion loss and the sensitivity with the IF cards excluded.

The conversion loss measurement was carried out at the FOI radar roof top lab. A 94 GHz +18 dBm RF signal was transmitted using a 25 dB rectangular horn located at a distance of R = 60 m from the receiver array. A 92.4 GHz +18 dBm LO source illuminated the FPA chip using the scalar horn mentioned above. The bias voltages were chosen for optimum SNR (gate and drain bias was –0.50 V and 2.5 V, respectively). The measured IF power levels are given in Table 2 and 3. The left side channel number one is in the topmost row and far right column on the left chip while the right side channel number one is the topmost row to the left on the right chip in Fig. 2.2.1, channel number two is in the second inner column etc.

By using the earlier calculated value for the reflector antenna gain, 42 dB [2], the mixer conversion loss, L, can be calculated (an IF loss of 1 dB has been assumed). Because of a design

flaw the conversion loss is about 3 dB higher for the right chip. The obtained conversion loss was found to vary between 9.8 dB and 16.5 dB (an average of 13.2 dB). This is a significant increase of the conversion loss of around 10 dB when compared to earlier measurements on the system [4] and is believed to be explained by the following: (1) The final stage of the LO chain was malfunctioning so it was omitted which reduced the LO power from +23 dBm to +19 dBm. (2) The waveguide loss from the LO source to the scalar antenna has increased because several short waveguide sections were connected together (+15 dBm was measured at the input to the antenna). (3) The polarization and distance of the LO antenna has changed.

With assumed gain values for the scalar horn and the patch antenna of 18 dB and 5 dB, respectively, the calculated value of the incident LO power into the mixer is -12 dBm, which according to breakout circuit measurements (2x25 μm device, see Chapter 3) would give a 14 dB conversion loss in a 50 Ω system and a couple of dB better conversion with the antenna as a source, i.e., about 12 dB which is in good agreement with what was measured (the average).

Channel	**P_{IF} [-dBm]**	**L [dB]**
1	33.8	10.3
2	33.7	10.2
3	33.5	10.0
4	34.2	10.7
5	35.2	11.7
6	33.2	9.7
7	34.2	10.7
8	34.2	10.7
9	33.5	10.0
10	34.2	10.7
11	34.2	10.7
12	35.5	12
13	36.7	13.2
14	35.5	12
15	35.0	11.5
16	N/A	N/A
Average	***34.4***	***10.9***

Table 2. Measured IF power level and conversion loss factor for left chip.

Channel	P_{IF} [-dBm]	L [dB]
1	35.3	11.8
2	36.5	13.0
3	37.5	14.0
4	37.3	13.8
5	36.0	12.5
6	35.5	12
7	40.0	16.5
8	38.8	15.3
9	35.3	11.8
10	36.5	13.0
11	37.5	14.0
12	39.3	15.8
13	35.3	11.8
14	36.5	13.0
15	39.3	15.8
16	38.3	14.8
Average	***37.2***	***13.7***

Table 3. Measured IF power level and loss factor for right chip

The sensitivity of the system was determined by reducing the RF power using an attenuator such that the estimated received RF power was –79 dBm. This corresponds to what would be received in our radar (10 W transmitter, transmit antenna gain of 30 dB) from a target having a radar cross-section (rcs) of 1 m^2 when measured on a distance of 500 m. By inserting an IF amplifier (G = 23 dB, NF = 4 dB) in front of the spectrum analyzer (HP8563E, NF ≈ 25 dB @ 1.6 GHz, RBW = 1 MHz) its influence on the noise floor is limited to approximately 2 dB.

The SNR was measured for four channels, two for each chip, randomly selected. The results are shown in Table 4. The rightmost column shows the (calculated) SNR that would be obtained for an rcs of 1 m^2 at a distance of 500 m and a measurement bandwidth of 50 MHz (taking into consideration the noise factor of the amplifier and spectrum analyzer). The first column shows, after subtracting the amplifier gain, that the minimum detectable signal into the IF-card is in the range of –90 to –85 dBm.

Channel	P_{IF} [dBm]	P_{noise} [dBm]	SNR_{raw} [dB]	SNR [dB]
9 (Left)	-67.0	-80.8	13.8	*2.8*
7 (Left)	-65.0	-80.0	15.0	*4*
13 (Right)	-67.5	-80.5	13.0	*2.0*
6 (Right)	-64.0	-80.8	16.8	*5.8*

Table 4. Measured sensitivity of the system

The calculated average SNR is 3.6, which is a decrease of roughly 7 dB compared with previous measurements that were made using a higher LO power (including the final LO stage). This SNR has turned out to be sufficient for the measurement purpose we have but it is nevertheless of interest to increase the LO power - and/or reduce the power requirement. One way to do the former is to purchase a new final stage injection-locked amplifier (ILO), while the latter e.g. could be realized by increasing the efficient antenna area for each pixel, see Chapter 4.2.

3. RF front-end

The RF front-end for the present system is based on integrated patch antennas that receives both RF and LO (in different polarizations) that are fed to an MMIC active gate mixer. In the next sections the design and characterization of this new mixer is described in more detail.

3.1. Novel active gate mixer MMIC

The gate mixer has many advantages as a mixer because both RF and LO are amplified and when the ratio $F_t/F_s>1$ it is possible to obtain gain from the mixer. The noise figure is also very good. A problem associated with the gate mixer is how to apply the RF and LO signals without losses. A common way is to use a directional coupler or a ring filter as a diplexer and another way is to use a balanced approach. However, both approaches add losses to both RF and LO. This problem can be alleviated if we distribute the LO quasi-optically. Here we use a dual-polarized patch antenna, but this is not a necessity. The RF and LO are in this case extracted from the neighboring sides of the patch and combined at the gate of the mixer. Since both the RF and LO are applied with small losses and a single FET device is used for each sensor, this circuit is attractive for use in our imaging application. This novel mixer was first investigated experimentally as a 1: 8 scale model at 12 GHz and showed a great reduction of the LO power requirement. A W-band MMIC mixer was then designed using the same approach for use in our millimeter-wave imaging sensor array.

The W-band MMIC mixer was first designed and manufactured using a 2x15 μm device and resulted in reductions in both the LO power requirement and the conversion loss (compared to the previously used resistive mixer). Further improvements were obtained by going for a larger (2x25 μm) device.

3.2. The device modeling (first generation, 2x15 μm device)

Philips Microwave, Limeil, France manufactured the MMIC mixer, using their D01PH process. A 0.15 μm GaAs device of width 2x15 μm was selected and the Chalmers nonlinear model was used in the mixer simulations.

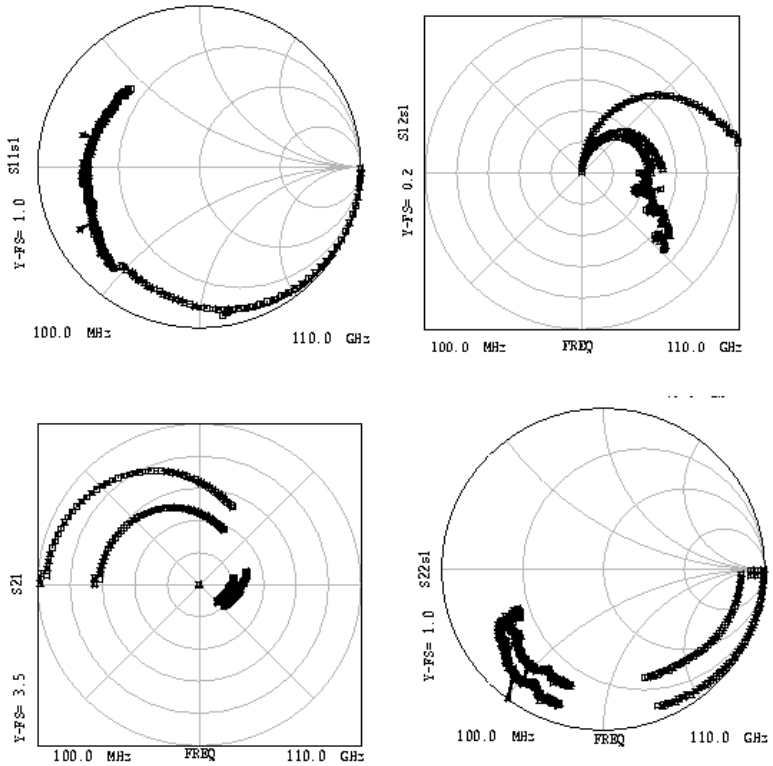

Fig. 3.2.1. Measured and modeled S-parameters of the transistor. V_{ds} = 2V and V_{gs} = -1V; -0.2V; 0V.

The device was measured at DC and S-parameters were obtained for the frequency range 0.1-110 GHz. From these measurements the large signal model was extracted. Special attention was paid to the accuracy of the capacitance part of the model. Later the model was evaluated with a power spectrum measurement. Measured and modeled S-parameters are shown in Fig. 3.2.1 using the Chalmers model [6] parameters as listed in Table 5.

I_{pks} mA	V_{pks} V	V_{pk0} V	P_{1s} 1/V	P_{10} 1/V	P_2 $1/V^2$	P_3 $1/V^3$	l 1/V	a_s 1/V	a_r 1/V
13.5	0.15	-0.05	2.1	3.5	-1.4	1.5	0.12	2.2	0.5
C_{gs} fF	C_{gd} fF	C_{ds} fF	R_g W	R_d W	R_s W	R_i W	L_g pH	L_d pH	L_s pH
25	9	10	5.5	9	9	8	3.5	3.5	2.5

Table 5. Philips, 0.15 μm x 2 x 15 μm, D01PH; V_{ds}=2 V,V_{gs}=0 V.

3.3. Mixer description

The layout of the MMIC mixer is shown in Fig. 3.3.1 and the layout of the single sensor element used for the HFSS calculations is shown in Fig. 3.3.2. The LO and RF are applied in different polarization and combined at the gate input pad of the mixer. The 94 GHz patch antenna with IF

and DC circuits are manufactured using an MCM-D (MultiChip Module – Deposited) process based on BenzoCycloButhene (BCB) at ACREO AB, Norrköping, Sweden. The multi-layer structure provides an easy interconnection between the layers where V_{ds}, V_{gs} and IF lines are routed in separate layers. The low dielectric constant, $\varepsilon_r = 2.7$, of the relatively thick layers of BCB, 3x15 μm, makes the efficiency of the antenna high. The gain of the patch antenna was previously measured and calculated to be approximately 5 dB. The input impedance of the antenna is transformed to the input of the MMIC using a filter structure consisting of the high impedance line attached to the patch, the bonding pad and the bond wires (n = 3).

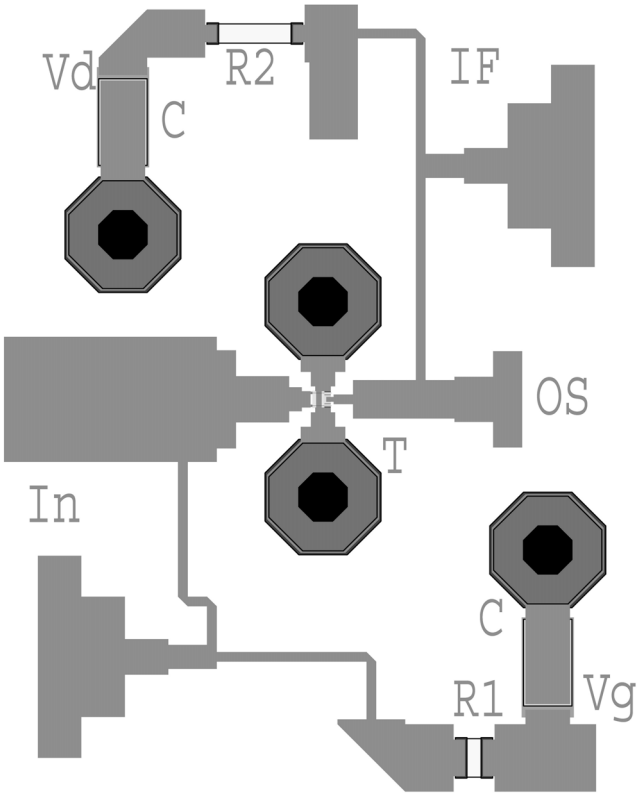

Fig. 3.3.1. Shows gate mixer MMIC layout. C = 2 pF, $R_1 = 50\ \Omega$ and $R_2 = 800\ \Omega$. Chip size is 1 mm x 1 mm.

The remaining part of the gate matching circuit is placed at the MMIC part. The gate and drain voltages are applied via resistors, R_1 and R_2, which also stabilize the mixer at low frequencies. At the drain side an open stub, OS, is used to provide a short circuit for the RF and LO frequencies and thus to maximize the current swing.

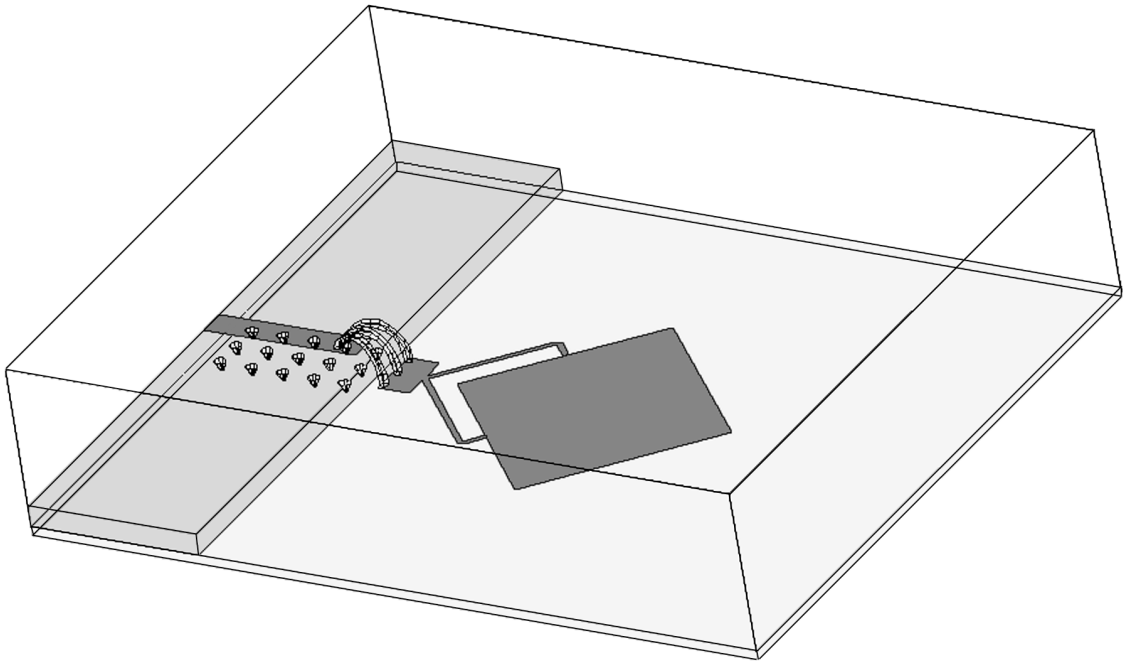

Fig. 3.3.2. Antenna circuit simulated using HP HFSS.

The circuit was designed using HP MDS and Ansoft Serenade and the antenna part including feed lines, bond pad and - wires and transition to the MMIC substrate was simulated using HP HFSS (see Fig. 3.3.2) and HP Momentum.

The small signal gain that can be obtained from the device is rather small (approximately 3 dB), but it can nevertheless operate quite well as a mixer. The conversion gain, G_c, from the mixer can be estimated as

$$G_c = \frac{g_{m,\max}^2 R_L}{16\omega_s^2 C_{gs}^2 \left(R_s + R_g + R_i\right)} \qquad \text{(E.5)}$$

where $g_{m,\max}$ is the peak transconductance and R_L is the IF load resistance.

3.4. Characterization of the new mixer

A mixer breakout circuit was used for impedance measurements and to establish fundamental properties of the mixer before characterizing the complete sensor including the antenna. The breakout circuit illustrated in Fig. 3.4.1 has a 50 Ω microstrip line feeding the mixer instead of the patch antenna.

The MMIC mixer was glued on the MCM structure and wire bonded to the patch, DC and IF bond pads. External coupling and decoupling capacitors were mounted close to the MMIC.

Calibration was done using a HP8510XF millimeter-wave vector automatic network analyzer (VANA) and W-band waveguide probes (Picoprobe) and a 50 Ω microstrip TRL cal kit manufactured on 45 μm BCB.

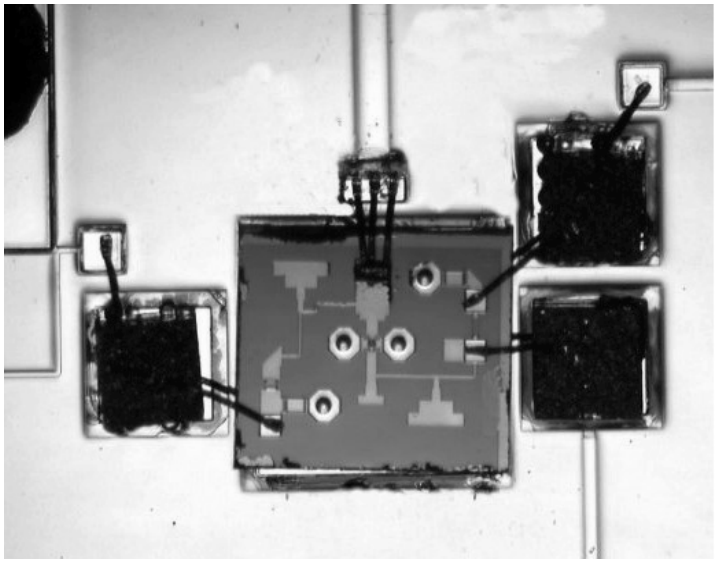

Fig. 3.4.1. Photo of mixer breakout circuit with the 50 Ω microstrip feed line (top). The MMIC is wire bonded, using n = 3 17 μm Au bond wires for the gate contact.

The measured mixer input impedance, Z_M, including the bond pad on BCB and three approximately 300 μm long bond wires is compared with simulated results (Libra) in Fig. 3.4.2. The reference plane is located at the upper edge of the 250 μm x 150 μm gate bond pad shown in Fig. 3.4.1.

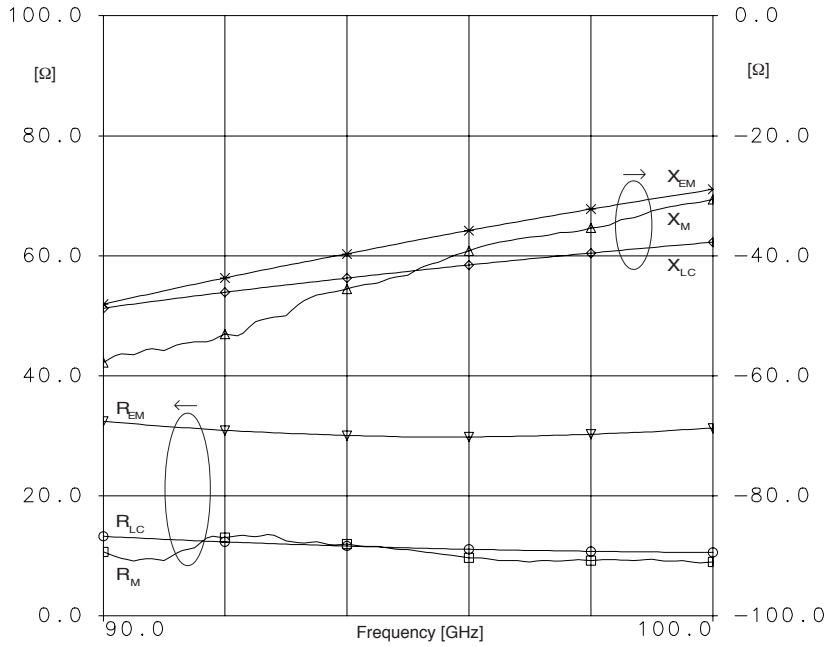

Fig. 3.4.2. Mixer input impedance, Z = R+jX. Z_M is measured, Z_{EM} and Z_{LC} are simulated using the Chalmers HEMT model in combination with, respectively, HFSS simulations and an LC-section for modeling of the bond wire transition.

Because the bond wire transition has a significant influence on the input impedance and thus the mismatch loss, this transition was modeled separately using HFSS. The obtained 2-port scattering matrix for a structure similar to the one illustrated in Fig. 3.3.2 but without the antenna and its feed lines was used together with the simulated MMIC input impedance to obtain the input impedance at the bond pad, Z_{EM} in Fig. 3.4.1. The correspondence in the imaginary part is excellent but the real part deviates notably from what was measured. It was found that a simple LC-section was able to model the bond wire transition between the BCB side and the MMIC in a better way, see Z_{LC} in Fig. 3.4.2. The capacitance C (located on the BCB side) and the inductance L of the LC-section were 47 fF and 100 pH, respectively.

The effect of the number and type of bond wires was investigated by measuring the impedance for different bond wire transitions. A reduced mismatch loss was confirmed (as anticipated) when increasing the number of bond wires from two to three and when replacing two bond wires with a ribbon bond. The results obtained from these measurements are shown in Fig. 3.4.3.

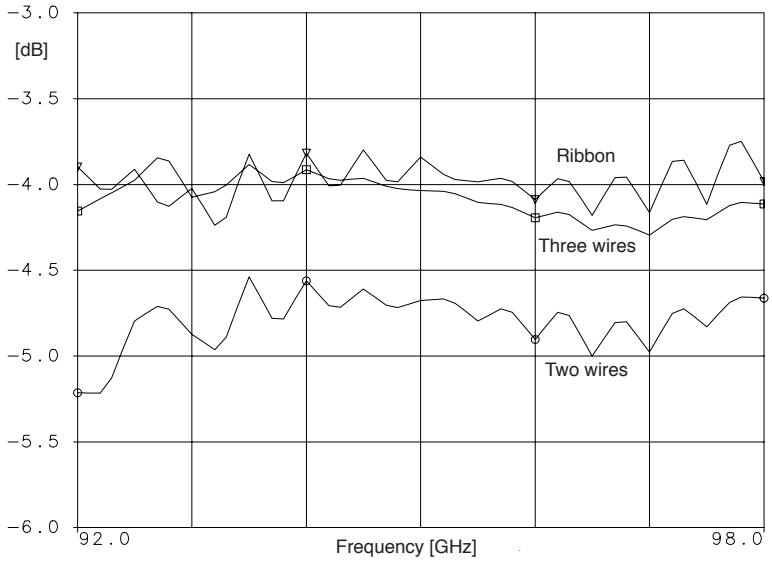

Fig. 3.4.3. Mismatch loss measured at the mixer input bond pad for three different bonding schemes. The bond length was approximately 300 μm for all three cases. The bond ribbon width was 125 μm.

The conversion loss for the mixer breakout circuit was measured and simulated as a function of LO power as illustrated in Fig. 3.4.4. The optimum DC bias was simulated to be V_{ds} = 2.5 V and V_{gs} = -0.15 V, while the experimentally found optimum is V_{ds} = 2.5 V and V_{gs} = –0.35 V. The simulated data was obtained using the Harmonic Balance (HB) technique and the Chalmers non-linear HEMT model. The LO and RF frequency was 92.5 and 94.5 GHz, respectively. The difference between measured and calculated (minimum) conversion loss for the mixer breakout circuit is explained by the fact that the measured and simulated mismatch loss differ; it is 1-2 dB for the simulated mixer but approximately 4 dB according to the measurements (using three bond wires as shown in Fig. 3.4.3).

The frequency response of the MMIC was measured for the mixer breakout circuit and is plotted in Fig. 3.4.5, which also contains the simulated frequency response for the MMIC. The LO frequency was 92.5 GHz and the LO power was 1 dBm.

The simulated MMIC frequency response is rather broadband and that is why the frequency response of the sensor is determined mainly from the patch antenna frequency response.

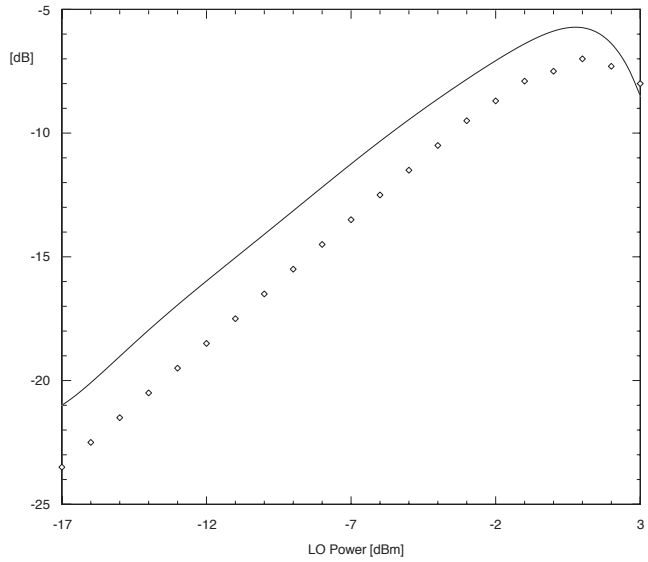

Fig. 3.4.4. Measured (diamonds) and simulated (solid line) conversion loss vs. LO power for the mixer breakout circuit.

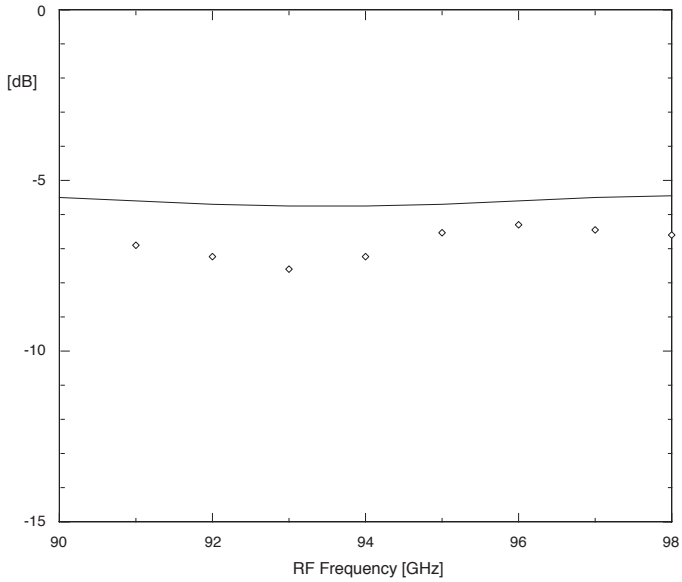

Fig. 3.4.5. Measured (diamonds) and simulated (solid line) conversion loss vs. RF frequency for the mixer breakout circuit.

The simulated RF and LO leakage to the IF output was between -32 dB and -54 dB and the measured leakage is plotted in Fig. 3.4.6.

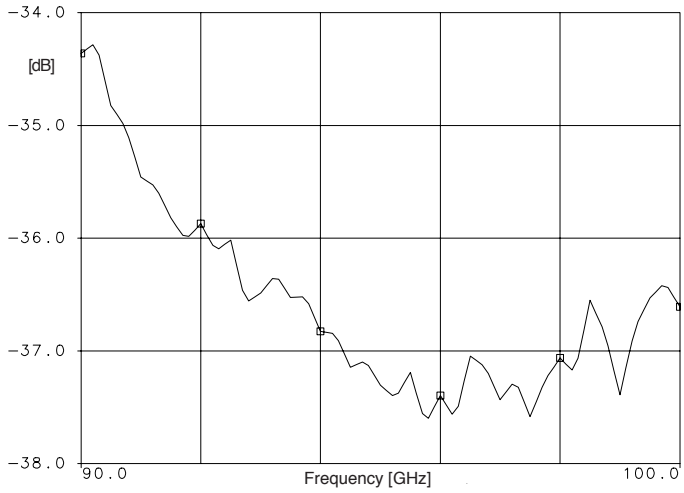

Fig. 3.4.6. Measured leakage from mixer input to IF output.

3.5. Experimental evaluation of the new sensor

The new sensor element based on the active gate mixer MMIC and a microstrip patch antenna receiving the RF and LO signals quasi-optically in orthogonal polarizations is shown in Fig. 3.5.1. The dimensions of the patch antenna are 952 μm x 934 μm and the supporting BCB thickness is 45 μm. The Cu metal thickness is 2 μm.

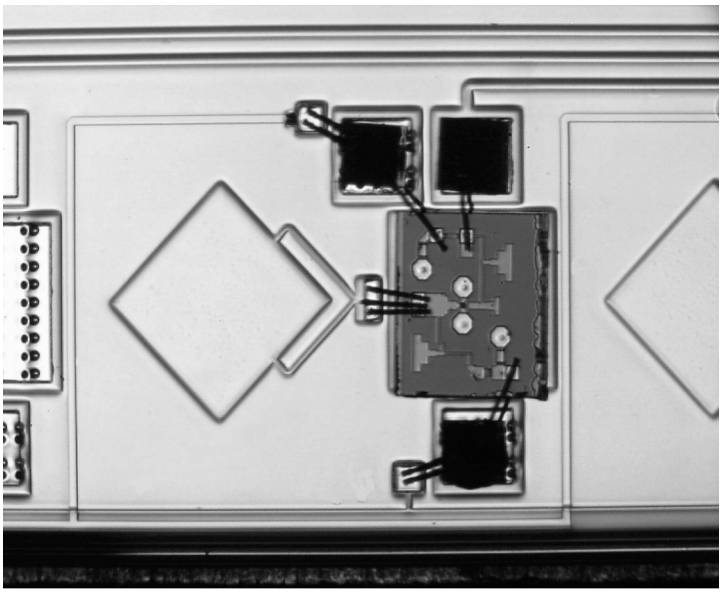

Fig. 3.5.1. Close-up photo of the new sensor element.

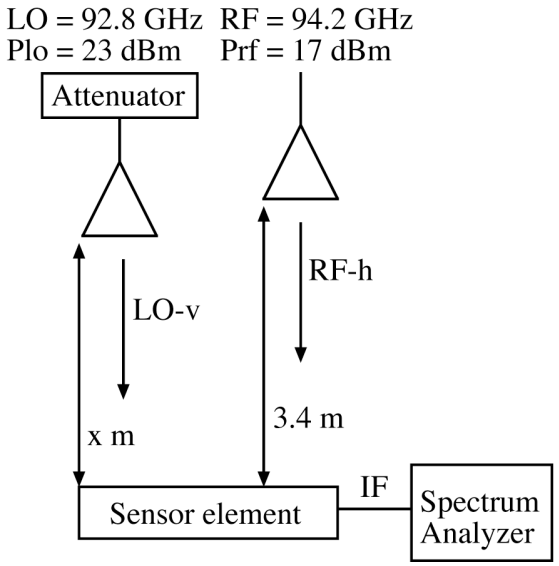

Fig. 3.5.2. Simplified schematic of the measurement set-up.

The conversion loss of the complete sensor element, see Fig. 3.5.2, was obtained by positioning the sensor in the far-field (3.4 m) of a horizontally polarized 26 dB horn antenna, which was connected to a 94.2 GHz RF source with output power +17 dBm. A 92.8 GHz LO source with output power ≤ 23 dBm adjustable using an attenuator was simultaneously illuminating the sensor element through a vertically polarized open waveguide positioned close to the sensor, at an angle to minimize the RF blockage. The IF output of the sensor was amplified and measured using a spectrum analyzer as a function of the LO power. A second measurement was made with the LO antenna moved to the far field of the sensor to establish an accurate relation between received LO power and conversion loss. The measured conversion efficiency for the new millimeter-wave sensor as a function of the calculated received LO power (assuming a constant antenna gain) is plotted in Fig. 3.5.3 together with results for sensors based on resistive mixers. Circles and triangles correspond to sensors based on the resistive HEMT mixer with and without pre-matching, respectively, using V_{gs} = -0.15V and V_{ds} = 0V. Squares correspond to the new sensor based on the active MMIC gate mixer using V_{gs} = -0.35V and V_{ds} = 2.50V ($I_{ds} \approx 2$ mA). The calculated received RF power was approximately –35 dBm.

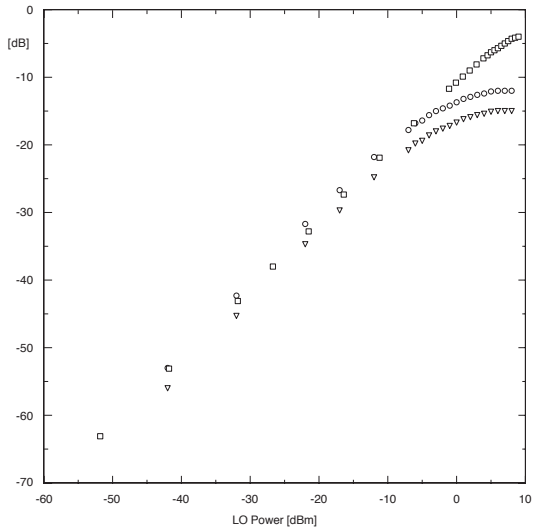

Fig. 3.5.3. Measured conversion efficiency vs. LO power for the 2x15 μm active gate mixer MMIC (squares) and a resistive HEMT mixer with (circles) and without (triangles) pre-matching, respectively.

The minimum conversion loss for the new sensor was estimated from the measurements to be between 4 and 5 dB. This is a couple of dB better than what was obtained for the mixer breakout circuit, which is explained by the fact that the antenna source impedance constitutes a better match than 50 Ω. At 94.2 GHz the measured mismatch loss is approximately 2 dB for the antenna-integrated sensor compared to approximately 4 dB for the breakout circuit (see below).

The frequency response of the sensor is mainly determined by the mismatch loss between mixer and antenna and by the frequency dependence of the antenna broadside response for the two used polarizations. Both the antenna impedance and the appropriate radiation patterns were obtained theoretically using the electromagnetic simulator HP Momentum. The calculated antenna impedance, Z_A, is plotted in Fig. 3.5.4. Fig. 3.5.5 shows the normalized antenna broadside response for the two polarizations, and the calculated mismatch loss using the theoretical antenna impedance, Z_A, and, respectively, (a) the measured mixer impedance Z_M, (b) the calculated mixer impedance Z_{LC}, and (c) the calculated mixer impedance Z_{EM}.

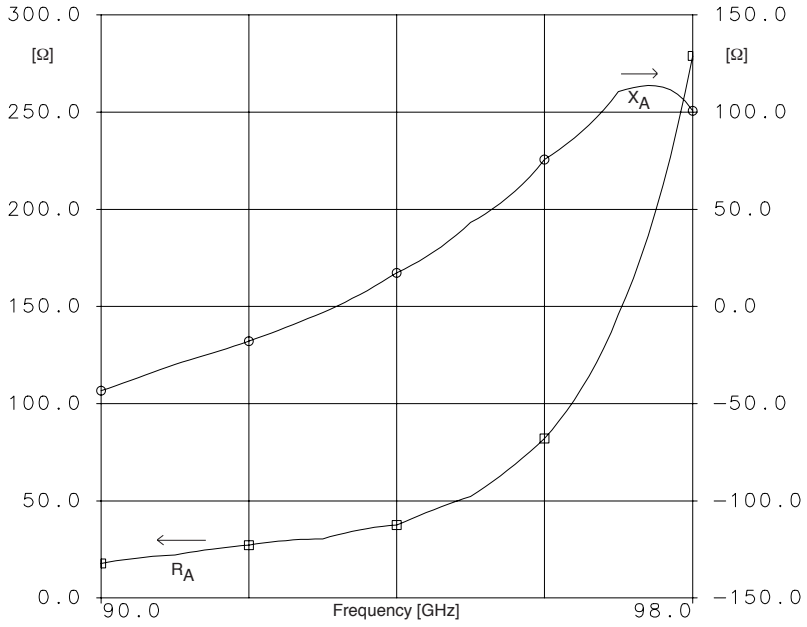

Fig. 3.5.4. Antenna impedance, Z_A, calculated with the reference plane located at the point where the two feed lines join at the bond pad.

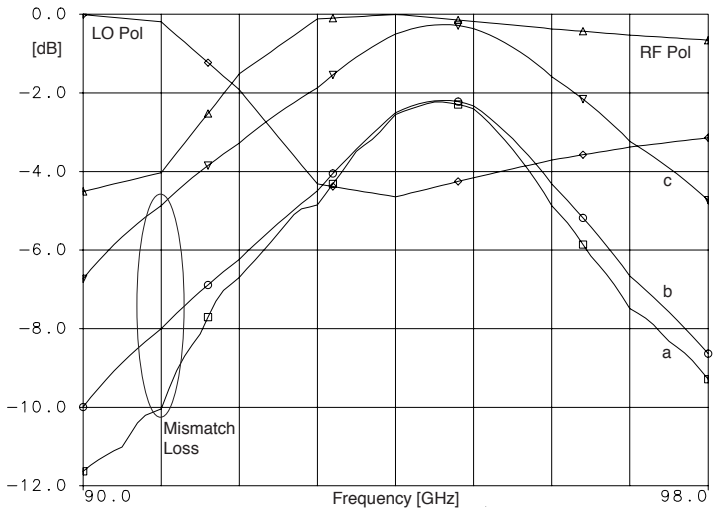

Fig. 3.5.5. Shows calculated broadside RF and LO polarization response and calculated mismatch loss between the calculated antenna impedance, Z_A, and the mixer impedances (a) Z_M, (b) Z_{LC}, and (c) Z_{EM}.

Fig. 3.5.6 shows the normalized measured RF frequency response for the sensor obtained by monitoring the IF power as the RF frequency was varied. The received LO power and frequency was kept at approximately 0 dBm (calculated) and 92.8 GHz, respectively. The normalized calculated RF frequency response obtained using the RF polarization response and a mismatch

loss calculated according to cases (a) - (c) are also plotted in Fig. 3.5.6. The agreement between the measured and simulated RF frequency response is good, particularly for (a) and (b) which use more or less measured data for the mixer breakout circuit input impedance. The RF frequency response has a sharp peak between 94 and 95 GHz, which is caused by a minimum mismatch loss and a maximum RF polarization response both located in this frequency range.

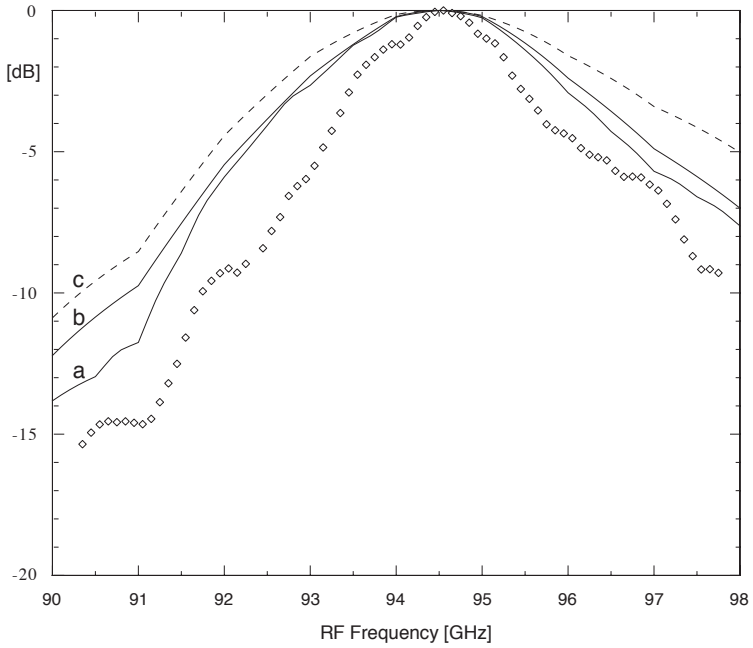

Fig. 3.5.6. Shows RF frequency response for the antenna-integrated sensor. Diamonds denote measured data and (a)-(c) denote data obtained using a mismatch loss according to the three cases in Fig. 3.5.5.

Fig. 3.5.7 shows the normalized measured frequency response for the new sensor obtained by monitoring the IF output power as the LO frequency was varied. The received RF power and frequency was kept at approximately –43 dBm (calculated) and 94.0 GHz, respectively.
The normalized frequency responses calculated using data from Fig. 3.5.5 are also plotted. The agreement between the measured LO response and the simulated response are reasonably good for case (a) (above 91 GHz) that uses the measured mixer impedance, Z_M. The measured LO response demonstrates two peaks; one caused by the minimum mismatch loss obtained in the frequency range between 94 and 95 GHz and a second peak between 91 and 92 GHz caused by the LO polarization response.

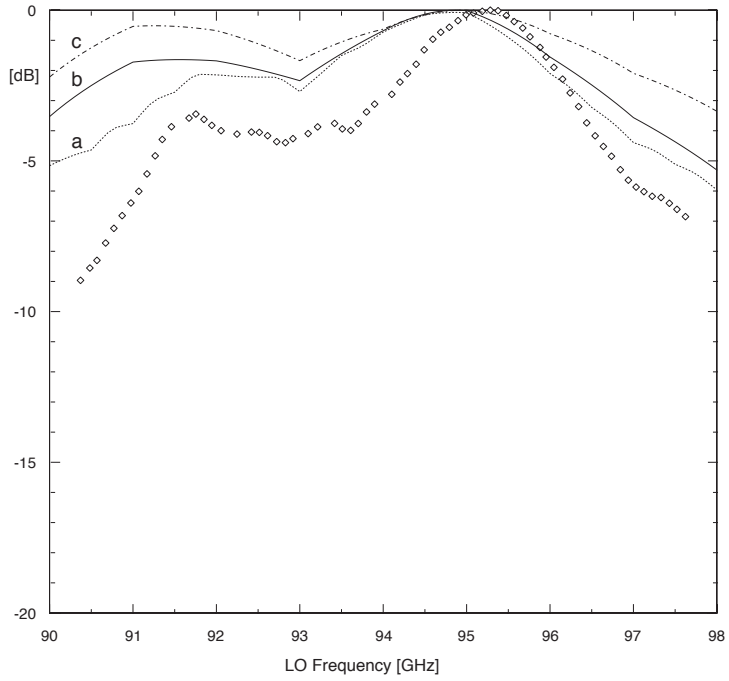

Fig. 3.5.7. Shows LO frequency response for the new sensor. Diamonds denote measured data and (a)-(c) denote data obtained using a mismatch loss according to the three cases in Fig. 3.5.5.

The minimum conversion loss was obtained for the sensor circuit using a calculated received LO power of between 8 and 9 dBm, which is 7-8 dB more pumping power than was required to saturate the mixer in the breakout circuit. This is caused by a mismatch loss of 5 dB and a LO polarization response which is down by 4 dB at 92.8 GHz (the polarization plane has rotated). This adds up to 9 dB, which is 5 dB more than the mismatch loss for the mixer breakout circuit and does explain the increased LO power required for this sensor.

The required LO power for the new mixer is reduced by approximately 7 dB when compared with the pre-matched resistive HEMT mixer and the minimum conversion loss is significantly lower.

3.6. Second generation mixer MMIC (2x25 μm device)

A second version of the active gate mixer MMIC was designed using a larger device, 2x25 µm, which according to simulations should decrease the LO power requirement further. After

manufacturing and delivery the mixer input impedance was measured using the same breakout circuit as described above.

Because the mixer must be matched at a certain bias and LO power level and the input impedance depends on all these it is first necessary to measure the mixer conversion loss as a function of these parameters to establish the optimal biasing condition.

The optimal incident LO power level for this mixer was found to be approximately 0 dBm, rather independently of the bias voltages. This is significantly lower than for the first generation of the active gate mixer MMIC, which saturated around +10 dBm. Using this LO power the optimal gate bias voltage was determined for different drain bias voltages. The optimal bias voltage for 0 dBm and –10 dBm incident LO power was {Vg = -471 mV; Vd = 5.0 V} and {Vg = -514 mV; Vd = 2.5 V}, respectively. The measured conversion loss for this bias condition as a function of LO power is plotted in Fig. 3.6.1.

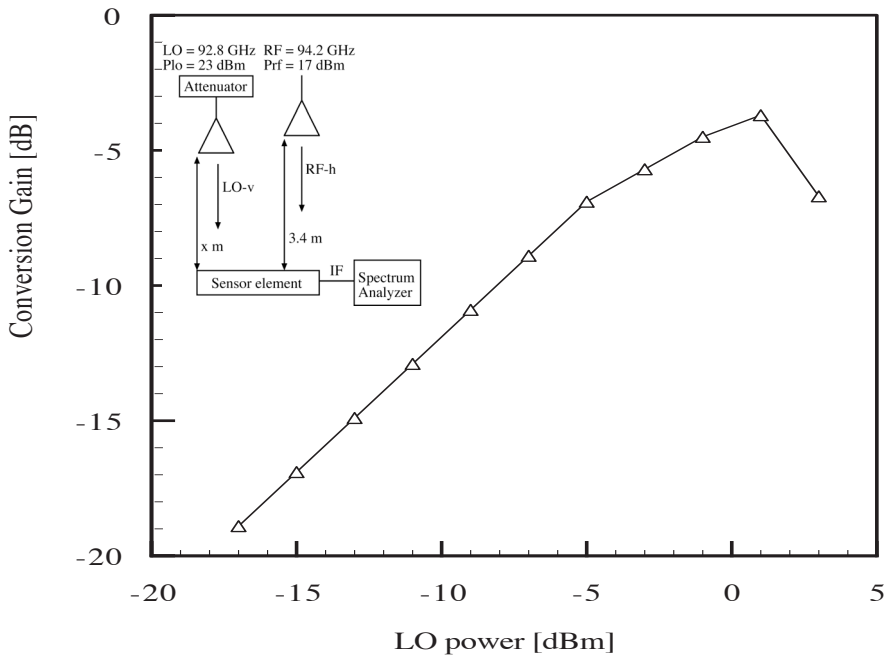

Fig. 3.6.1. Measured conversion loss for the 2x25 μm version of the new mixer.

The minimum obtained conversion loss in a 50 Ω system is 3.7 dB which corresponds to approximately 0.5 dB after compensating for the mismatch loss at the RF frequency. Compared

to the first generation of this mixer it is an improvement by 4.7 dB – measured in a 50 Ω system. This is mainly attributed to the use of a larger device.

The measured conversion loss is an excellent result considering that the used MMIC process, OMMIC D01PH, has an f_T of only approximately 100 GHz.

In Fig. 3.6.2 the real and imaginary parts of the measured input impedance is plotted for two bias conditions as was measured using the HP8510XF VNA. The two bias conditions in the figure corresponds to the optimal conditions for two different values of incident LO power; -10 dBm and 0 dBm. Since the impedances are almost identical it is clear that the mixer can be matched to an antenna even if we don't exactly know the received LO power.

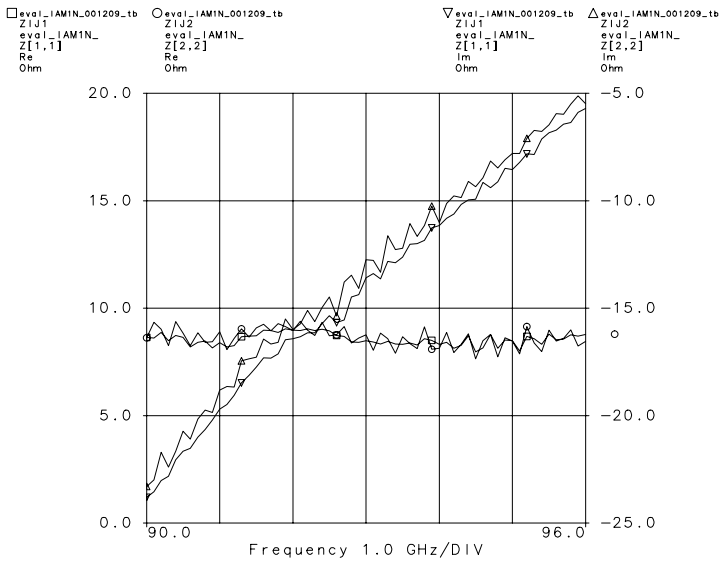

Fig. 3.6.2. Measured impedance for the 2x25 μm version of the new mixer.

4. New sensor designs

Further improvements of the sensor have been studied using alternative antenna concepts compatible with the used MCM process. The intention is to improve the sensor sensitivity in three steps; 1) reduced mismatch loss and 2) reduced spillover loss and 3) increased antenna efficiency and improved antenna diagrams.

4.1. Reduction of mismatch loss

The mismatch loss between the antenna and the mixer for the sensor described in Chap. 2 is higher than desired and can be reduced. The problem to accurately calculate the input impedance of the mixer including the bond wire transition can be avoided by designing an antenna using measured data for the bond wire/mixer combination. Such a design has been made using a single polarization for both RF and LO, illustrated in Fig. 4.1.1. To achieve the required match from 92.4 GHz to 94 GHz, which is shown in Fig. 4.1.2, a 'detuned' patch is used in combination with impedance transformers, see Fig. 4.1.1. Two chips are used for assembly of a 4x8 array.

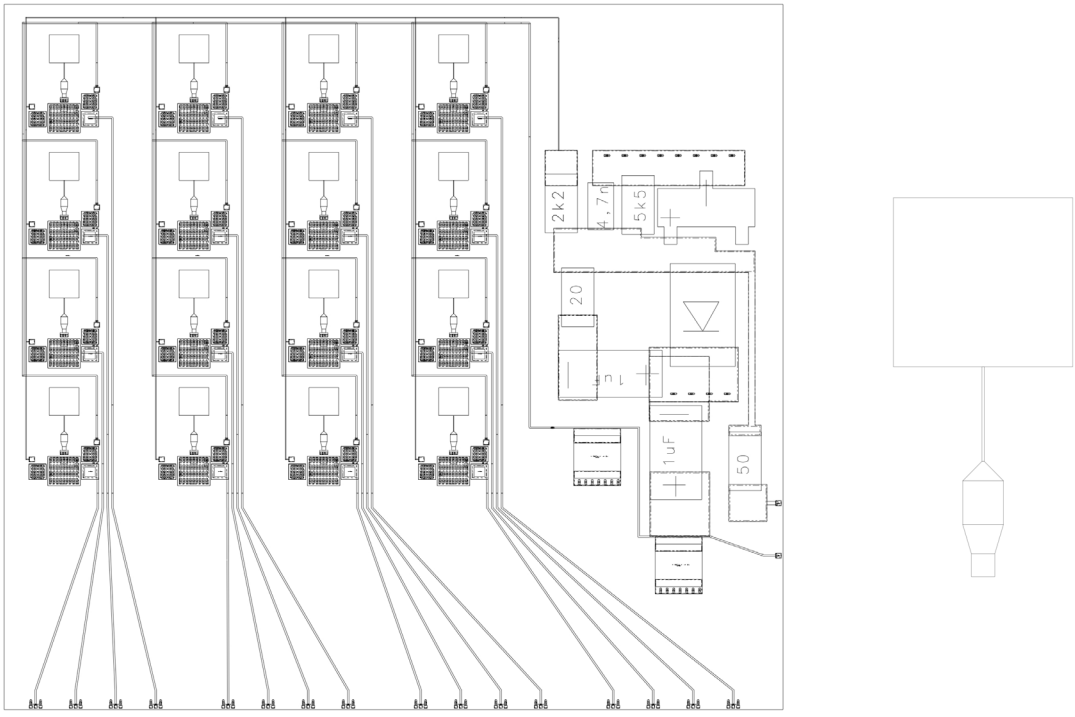

Fig. 4.1.1. Layout for new FPA (left) using a new antenna matching network (right).

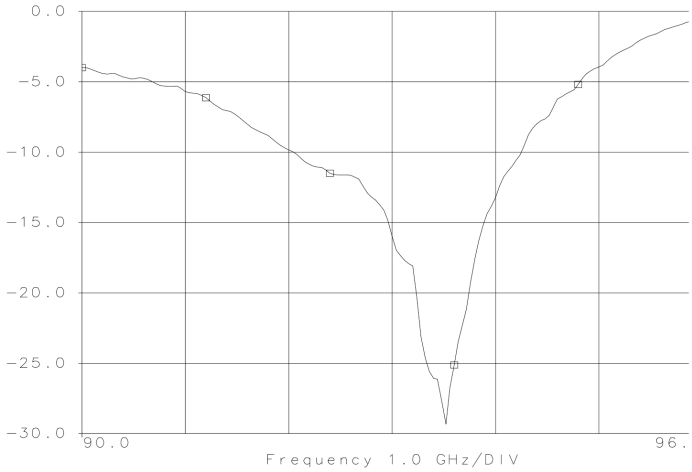

Fig. 4.1.2. Simulated reflection coefficient between antenna and mixer in Fig. 4.1.1.

4.2. Reduction of spillover loss

As was discussed in Chap. 2 one contribution to the total loss is spillover, i.e., the feed antenna beamwidth is larger than the opening angle of the reflector. The loss in this case is only a relative loss related to the fact that an unnecessarily low gain is used for the feed antenna (patch).

To overcome this a smaller F/D number could be used for the reflector, but this leads to higher scan loss. A better approach is to reduce the beamwidth of the feed antenna using subarrays of patch antennas. A 4x8 focal-plane array using 2x2 patch antenna subarrays as feed elements was designed for use with the second generation (2x25μm) active gate mixer MMIC, see layout illustration in Fig. 4.2.1.

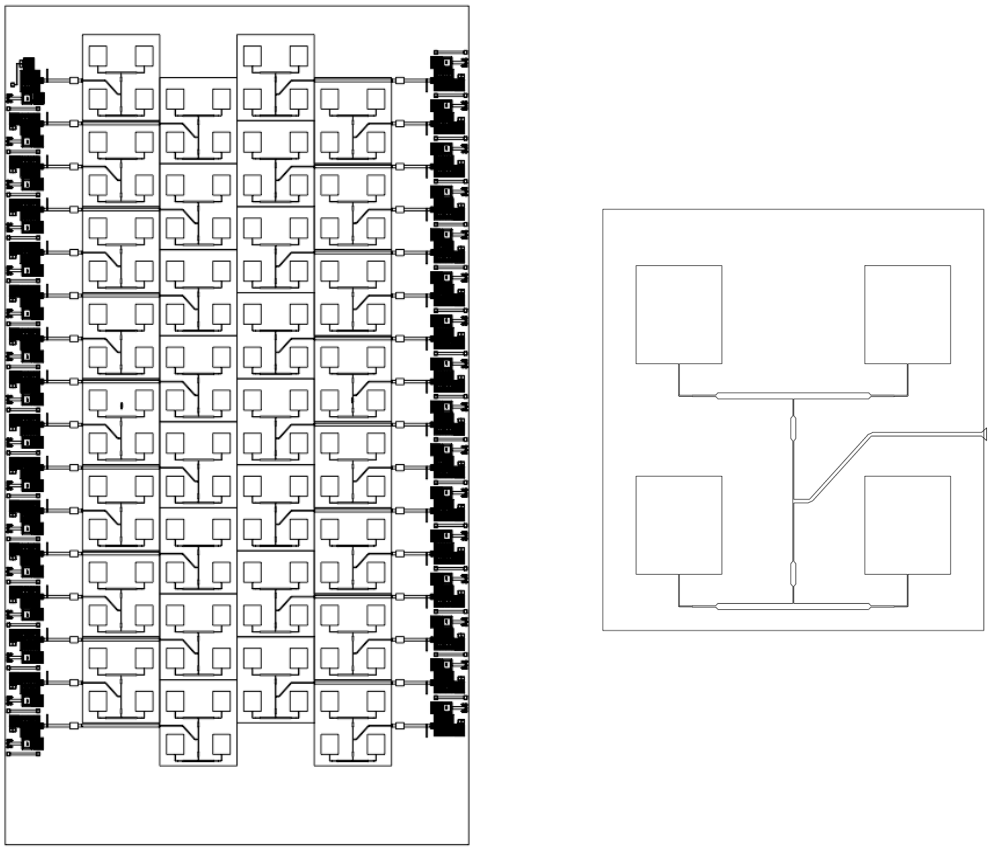

Fig. 4.2.1. Layout for 4x8 pixel focal plane array (left) using 2x2 patch subarrays as feed elements (right).

The 2x2 subarray feed uses a single polarization for reception of both RF and LO at 94 GHz and 92.4 GHz, respectively. This will also improve the link budget for the LO chain; less LO power will be wasted since the 2x2 antenna area is closer to the unit cell area compared to the single patch antenna case. Because the impedance bandwidth of a single patch antenna is smaller than the 1.6 GHz required to cover both RF and LO, the subarray uses a 'detuned' patch in combination with a feed network that includes several 'impedance transformers' (see Fig. 4.2.1) to achieve the required bandwidth. The simulated (HP Momentum) reflection coefficient of the subarray is plotted in Fig. 4.2.2. This array has a unit cell that is 4 mm x 4 mm and is designed for use with a 30 cm dielectric lens with a F/D number and beam deviation factor (BDF) that will permit diffraction limited field sampling at the Nyquist limit at 94 GHz. However, the use of a subarray for each pixel makes it necessary to mount the mixers external to the array; in this case at the boundary of the chip. The advantage is that the active devices can be somewhat shielded from the incoming fields and that undesired interference between mixers and antennas is

reduced. The disadvantage is the longer feed lines for some of the pixels and a potentially increased cross-talk. The latter was, however, investigated for several 2x2 pixel break-out circuits and found small. Bias network circuitry will be mounted off-chip for this design.

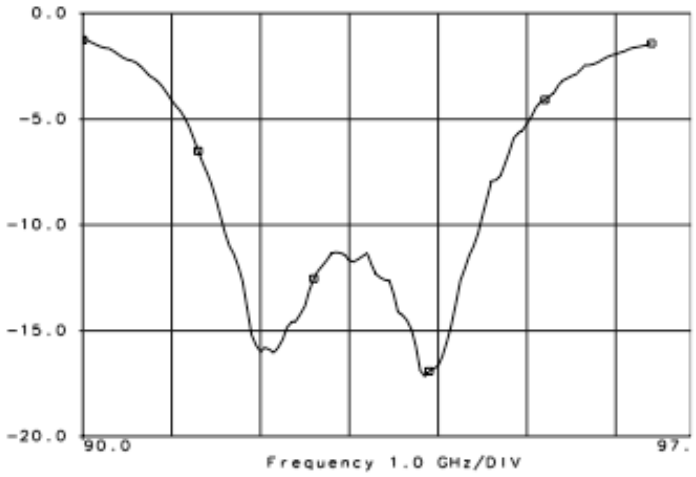

Fig. 4.2.2. Simulated reflection coefficient for the 2x2 subarray in Fig. 4.2.1.

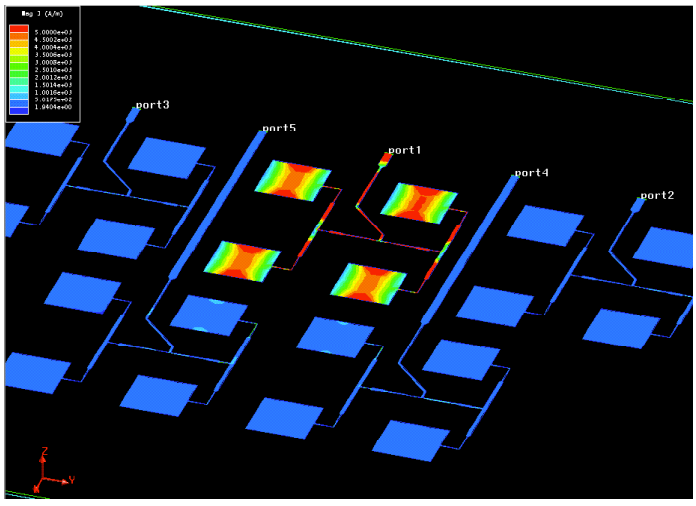

Fig. 4.2.3. Simulated surface current distribution using Ansoft Ensemble.

4.3. Increased antenna efficiency

The efficiency of the patch antenna in this application has previously been determined both experimentally and theoretically to roughly 50 %. To further improve the sensitivity of the radar system we need to decrease the losses of the feed antennas.

One approach that is compatible with the used MCM technology would be to manufacture dielectric resonator antennas (DRAs) on the backside of the Si wafer. To avoid increased dielectric losses we need to use a high-resistivity Si wafer. The DRAs could then be fed using aperture feeds from the BCB side of the MCM. By using 2x2 DRA subarrays matched to the mixer we could simultaneously reduce the mismatch loss, the spillover loss and the ohmic loss in the feed antennas. By locating the antennas and the circuits on different sides of the structure we will also improve the 'purity' of the antenna diagrams.

A focal-plane array was accordingly designed and simulated using Ansoft HFSS and Agilent ADS/Libra. The layout is illustrated in Fig. 4.3.1; blue indicates transmission lines or apertures and green is the backside Si after etching. The simulated antenna efficiency (HFSS) is about 70 %, which includes the loss in the 2x2 power distribution network.

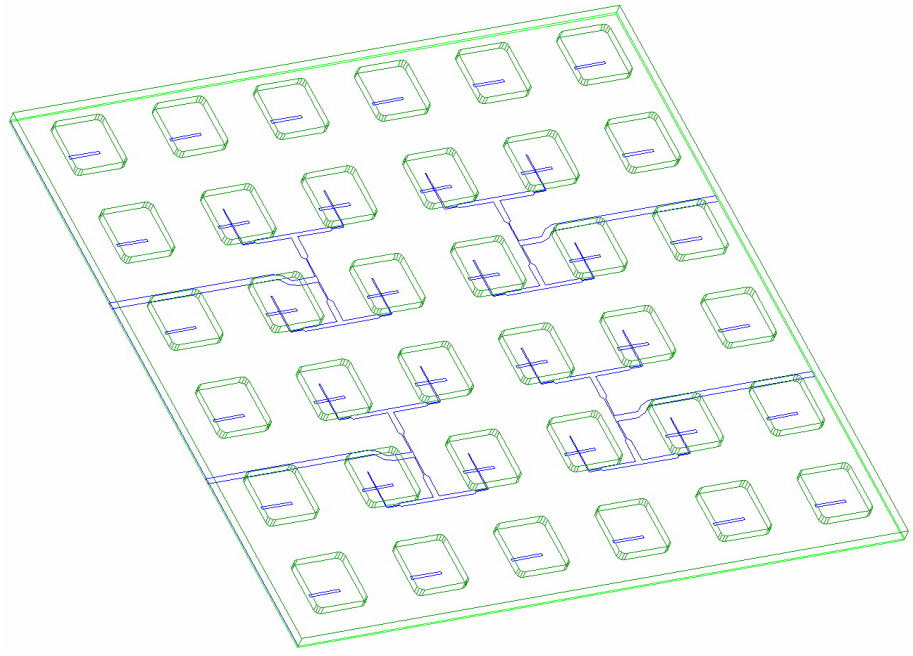

Fig. 4.3.1. Focal-plane array using aperture fed 2x2 DRA subarrays as feeds.

5. Summary and conclusions

Compared to an earlier developed radar (4x4 pixels) that used a front-end based on InP HEMT resistive mixers, the new 4x8 radar uses a new type of GaAs MMIC active gate mixers. This have improved the sensitivity such that the average SNR is 3 dB for a target with an rcs of $1m^2$ measured at a distance of 500 m using a 50 MHz bandwidth.

The sidelobe levels were earlier found acceptable even for the outermost element in the 4x8 array and always < -11 dB.

The IF circuitry was modified by manufacturing the diode detector matching circuitry on a separate Duroid substrate, which has a more well-defined permittivity than FR4. In this way the center frequency of the filter could be made much closer to the design frequency of 1.6 GHz.

However, since the current IF circuitry only allows incoherent detection new IF circuitry is being designed. The new design [5] will permit coherent detection and also increase the SFDR of the system much more than any modifications of the present IF circuitry.

6. References

[1] Ruthledge, D. B., et al, “Integrated-Circuit Antennas”, in Button, K. J. (Ed.*), Infrared and Millimeter Waves, Vol. 10, Millimeter Components and Techniques, Part II*. London Academic Press, 1983

[2] J. Svedin, “An Evaluation of Reflector Systems for Use with a 94 GHz Staring Receiver Array”, FOA Report FOA-D—95-00138-3.2—SE, June, 1995

[3] Yngvesson. K. S. “Near-Millimeter Imaging with Integrated Planar Receptors: General Requirements and Constraints”, in Button, K. J. (Ed.*), Infrared and Millimeter Waves, Vol. 10, Millimeter Components and Techniques, Part II*. London Academic Press, 1983

[4] J. Svedin, FOI Document no. 01-1463/L, April, 2001.

[5] J. Svedin, A. Gustafsson, S. Lindström, “Implementering av koherent detektion med mm-vågs mottagare” FOI Document Dnr. 03-2222, sept 2003.

[6] I. Angelov, L. Bengtsson, M. Garcia, “Extentions of the Chalmers Nonlinear HEMT and MESFET Model," *IEEE Trans. Microwave Theory Tech.*, vol. 44, no. 11, pp. 1664-1674, Oct. 1996.